

Research Paper

In vivo Imaging-Guided Nanoplatfom for Tumor Targeting Delivery and Combined Chemo-, Gene- and Photothermal Therapy

Cheng Li^{1*}, Xiao-Quan Yang^{1*}, Ming-Zhen Zhang^{2,3}, Yuan-Yang Song¹, Kai Cheng¹, Jie An¹, Xiao-Shuai Zhang¹, Yang Xuan¹, Bo Liu¹, Yuan-Di Zhao^{1,4}✉

1. Britton Chance Center for Biomedical Photonics at Wuhan National Laboratory for Optoelectronics-Hubei Bioinformatics & Molecular Imaging Key Laboratory, Department of Biomedical Engineering, College of Life Science and Technology, Huazhong University of Science and Technology, Wuhan 430074, Hubei, P. R. China
2. Institute of Medical Engineering, Department of Biophysics, School of Basic Medical Sciences, Xi'an Jiaotong University Health Science Center, Xi'an, Shaanxi, 710061, China
3. Digestive Disease Research Group (DDRG), Institute for Biomedical Sciences, Center for Diagnostics and Therapeutics, Georgia State University, Atlanta, GA, 30302, USA.
4. Key Laboratory of Biomedical Photonics (HUST), Ministry of Education, Huazhong University of Science and Technology, Wuhan 430074, Hubei, P. R. China

*These authors contributed equally to this article.

✉ Corresponding author: Tel/Fax: +86-27-8779-2202. Email address: zydi@mail.hust.edu.cn (Y.D. Zhao).

© Ivyspring International Publisher. This is an open access article distributed under the terms of the Creative Commons Attribution (CC BY-NC) license (<https://creativecommons.org/licenses/by-nc/4.0/>). See <http://ivyspring.com/terms> for full terms and conditions.

Received: 2018.07.01; Accepted: 2018.10.19; Published: 2018.11.10

Abstract

Currently, a large number of anti-tumor drug delivery systems have been widely used in cancer therapy. However, due to the molecular complexity and multidrug resistance of tumors, monotherapies remain suboptimal. Thus, this study aimed to develop a multifunctional theranostic nanoplatfom for effective cancer therapy.

Methods: Folic acid-modified silver sulfide@mesoporous silica core-shell nanoparticle was first modified with desthiobiotin (db) on the surface, then doxorubicin (DOX) was loaded into pore. Avidin was employed as "gatekeeper" to prevent leakage of DOX via desthiobiotin-avidin interaction. Db-modified survivin antisense oligonucleotide (db-DNA) which could inhibit survivin expression was then grafted on avidin at the outer layer of nanoparticle. DOX release and db-DNA dissociation were simultaneously triggered by overexpressing biotin in cancer cells, then combining PTT from Ag₂S QD to inhibit tumor growth.

Results: This nanoprobe had satisfactory stability and photothermal conversion efficiency up to 33.86% which was suitable for PTT. Due to the good targeting ability and fluorescent anti-bleaching, its signal still existed at the tumor site after tail vein injection of probe into HeLa tumor-bearing nude mice for 48 h. *In vitro* and *in vivo* antitumor experiments both demonstrated that drug, gene and photothermal synergistic therapy significantly enhanced antitumor efficacy with minimal systemic toxicity.

Conclusion: Our findings demonstrate that this novel nanoplatfom for targeted image-guided treatment of tumor and tactfully integrated chemotherapy, photothermal therapy (PTT) and gene therapy might provide an insight for cancer theranostics.

Key words: mesoporous silica, fluorescence imaging, photothermal therapy, gene therapy, drug delivery system

Introduction

Malignant tumor affects human health worldwide [1]. Although traditional chemotherapy still occupies a dominant position in clinical treatment, but

due to the side effects caused by nonspecific distribution of chemotherapeutic drugs, and a large number of tumors appear multidrug resistance, the

drawbacks of a single treatment mode are becoming increasingly apparent [2]. Therefore, multi-mode combination therapy is hopeful to conquer cancer in the near future.

In recent years, the development of nanobiotechnology has brought new ideas for cancer therapy. Fluorescence imaging, as one molecular imaging technology, has attracted much attention owing to its high sensitivity, high resolution and short acquisition time. Since it can detect the dynamic change of tumor-related molecule in real time, it has great application prospect in early diagnosis [3]. Ag₂S QD with emission in NIR-II region solves the interference of auto-fluorescence from tissue and blood during *in vivo* fluorescent imaging [4-6]. In addition, Ag₂S QD with 1.1 eV band gap also possesses ideal light absorption efficiency and high photothermal conversion efficiency, therefore, it could be used to achieve simultaneous fluorescence imaging and photothermal therapy (PTT) [7-10]. PTT as a rapid and efficient method for tumor therapy has attracted more attention, the photothermal agent has been used to convert the luminous energy into heat to make tumor regional hyperthermia (>41 °C), thereby killing tumor cell without damaging normal tissue through the difference of temperature tolerance between normal tissue and tumor tissue [11-13]. However, because of the uneven heat distribution of PTT, deep tumor treatment is insufficient and tumor is easy to relapse when used alone. Previous studies have shown that PTT can also increase cell membrane permeability and enhance the toxicity of chemotherapy drug, or trigger the immune response to inhibit tumor metastasis and recurrence [14-17]. Therefore, PTT combined with other therapy has become a promising method for efficient tumor ablation and minimally invasive treatment [18].

Many drug delivery systems have been established in the past years including liposome [19], polymer [20], inorganic nanoparticle [21] and protein nanocarrier [22]. Among these nanocarriers, mesoporous silica nanoparticle (MSN) has emerged as robust vehicle for drug delivery due to its high surface area, adjustable pore size, stable framework and excellent biocompatibility [23,24]. Zink and co-workers synthesized polymer-modified MSN for DOX delivery, achieved high-efficiency drug release at the tumor site *in vivo* [25]. In addition, the core-shell composite particles were prepared by coating mesoporous silica onto Fe₃O₄ [26], gold [27] or upconversion nanoparticle [28] cores, thus giving MSN more novel applications. Stimulus-responsive drug controlled release system is an intelligent transportation system which can respond to various external or internal stimuli, such as pH [29], redox

agent [30], enzyme [31], biomolecule [32], light [33] and temperature [27]. Easily modified MSN as an ideal stimulating response drug controlled-release platform, can be simultaneously assembled with stimulus-responsive moiety and targeting moiety. Biotin, also known as vitamin H, owing to the rapid propagation, vigorous metabolism and abundant mitochondria of tumor cell, the endogenous biotin content in tumor cell is significantly higher than that in normal tissue cell [34]. Remarkably, biotin can bind avidin with high specificity, and biotin-avidin system has been widely applied in biomedical fields. As a derivative of biotin, desthiobiotin also can bind avidin specifically, while its binding force is lower than that of biotin (dissociation constant $K_d=10^{-11}$ and 10^{-15} mol/L, respectively) [35].

Gene interference based on nucleic acid such as antisense oligonucleotide and small interfering RNA, has a broad application prospect in tumor therapy [21,36]. Survivin, an inhibitor of apoptosis protein is highly expressed in tumor cell and associated with chemotherapy resistance. Studies have shown that survivin acts on the junctions of various apoptosis pathways, directly inhibits the terminal effector protein Caspase-3 and Caspase-7, and prevents the apoptosis of tumor cell [37]. Anti-survivin therapy is an attractive cancer therapy strategy for its notable targeting, specificity and safety.

Hence, a novel multifunctional nanoplatform integrating fluorescence imaging/chemotherapy/thermotherapy/gene therapy (QD@M/D-Avidin/FA) was designed in this manuscript (Figure 1). Firstly, Ag₂S QD was coated with mesoporous silica to prepare core-shell composite particle (QD@M), alternatively, folic acid (FA) and desthiobiotin (db) were both modified on its surface to obtain targeting nanoparticle QD@M-db/FA. Followed, classic anti-cancer drug, doxorubicin (DOX), was adsorbed into the mesoporous silica pore, and "gatekeeper" avidin with a size slightly larger than the pore diameter [38] was combined with desthiobiotin to block drug leakage. Since one avidin molecule has four binding sites, desthiobiotin-modified survivin antisense oligonucleotide (db-DNA) could be linked on the probe surface *via* the desthiobiotin-avidin interaction to get QD@M/D-DNA/FA. After the targeting probe was preferentially taken up by tumor cell through receptor-mediated endocytosis, DOX release and db-DNA dissociation were simultaneously triggered to induce apoptosis and inhibit tumor growth. Here, Ag₂S QD was not only used to trace the transportation of nanoparticle *in vivo*, but also participated in PTT. Results indicated that this multifunctional nanoplatform had excellent biocompatibility and tumor targeting, and could effectively fight against cancer

under the synergistic treatment of chemo-, photo-thermal and gene therapy. This novel multifunctional theranostic nanoplatform provides a new idea for high efficiency treatment of malignant tumor.

Methods

Synthesis of hydrophobic Ag₂S QD

The synthesis of Ag₂S QD was modified according to the previous literature [13]. A given amount of 76.8 mg Ag (DDTC), 30 g ODE and 6 g DT were successively added into a four-necked flask (100 mL) under Ar protection. Then, water in the system was removed with vigorous stirring and heating to 90 °C for 10 min. The reaction was heated to 150 °C and quenched by *n*-hexane after maintaining the temperature for 10 min. The solution was cooled to room temperature, centrifuged and washed twice with acetone. The hydrophobic Ag₂S QD was re-dispersed in chloroform.

Synthesis of mesoporous silica encapsulated Ag₂S (QD@M)

0.2 g CTAB and 6 mg Ag₂S were dissolved in 10 mL water and homogenized with ultrasound. The mixture was heated to 70 °C and stirred rapidly to completely evaporate chloroform to obtain clear and transparent brown Ag₂S/CTAB dispersion system. Then 90 mL water and 3 mL ammonia were added, gently equilibrated at 40 °C for 2 h. Vigorous agitation

was carried out followed by rapidly adding 400 μL TEOS and 5 mL ethyl acetate to maintain 1 min, reduced the stirring speed and gently stirred for 6 h. The resulting QD@M was purified by repeated centrifugation (10000 rpm, 10 min) to remove the unreacted reagent by water and ethanol. The QD@M was re-dispersed in 50 mL ethanol containing ammonium nitrate (10 mg/mL) and heated to 75 °C for 6 h to remove CTAB template, the same purification methods were used as mentioned above.

Synthesis of QD@M-db/FA

In order to couple FA and db to the surface of QD@M, FA silane precursor and db silane precursor were prepared [28]. 15 mg FA or 7.28 mg db, 9.9 mg EDC and 9.9 mg NHS were dissolved in 10 mL DMSO followed by adding 20 μL APTES. The system was stirred for 8 h at room temperature to produce amino-functionalized FA or db silane precursor. Both precursors were mixtures containing FA or db coupled APTES and unreacted APTES, respectively. Then 100 mg QD@M was dissolved in 10 mL DMSO and further stirred for 24 h after mixing with above two systems. The final FA and db co-modified nanoparticle (QD@M-db/FA) was centrifuged (12000 rpm, 10 min) and washed twice with DMSO followed by washing 3 times with water. For control experiment, only db-functionalized silane precursor was added to obtain QD@M-db nanoparticle.

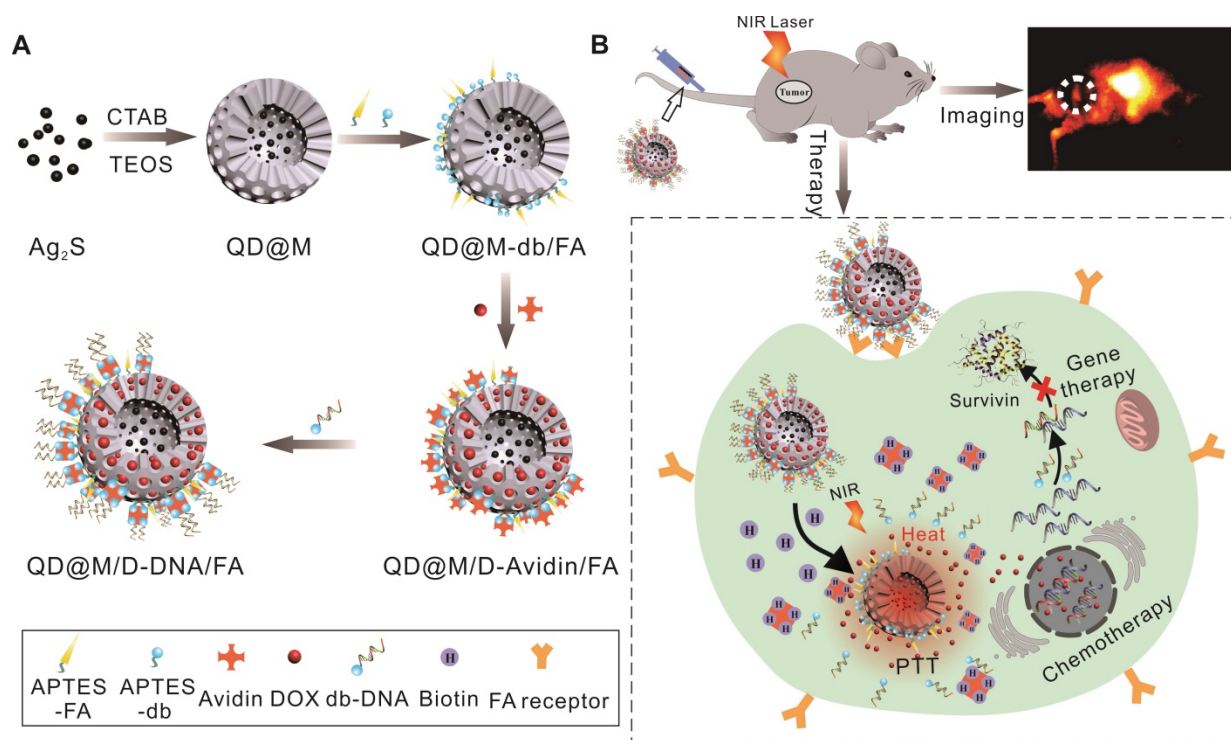


Figure 1. Schematic illustration of the synthesis route of QD@M/D-DNA/FA (A) and the tumor targeted fluorescence imaging and combined chemotherapy, photothermal and gene therapy (B).

DOX loading and db-DNA coupling

20 mg QD@M-db/FA and 2 mg DOX was added into 7 mL water. After stirring for 24 h, 1 mL avidin (1 mg/mL) was added and stirred for 2 h to cap the pore. The mixture was repeated centrifugation (12000 rpm, 10 min) with PBS (0.1 M, pH 7.4) to clean free DOX to obtain DOX-loaded nanoparticle (QD@M/D-Avidin/FA). FITC-loaded nanoparticle, QD@M/FITC-Avidin/FA was prepared by same protocol for flow cytometry, and DOX-loaded QD@M/D-Avidin without modifying FA was also prepared as control. 1 mg QD@M/D-Avidin/FA was added in 50 μ L hydrofluoric acid to dissolve mesoporous silica, and pH was adjusted to neutrality to determine DOX amount by analyzing fluorescence intensity at 590 nm. Loading content (%)=(DOX weight in probe)/(probe weight) \times 100% and encapsulation efficiency (%)=(DOX weight in probe)/(DOX initial weight) \times 100%. Then db-DNA was re-dispersed in QD@M/D-Avidin/FA at a final concentration of 1 μ M. The mixture was stirred for 2 h to obtain DNA-modified probe (QD@M/D-DNA/FA). Ag⁺ concentration was measured by graphite furnace atomic absorption method.

Photothermal effect and photothermal conversion efficiency

200 μ L QD@M at different concentrations (0-12 mg/mL and 0-200 μ g/mL) was irradiated with 808 nm laser (1.5 W/cm² and 2 W/cm²) for 5 min at a distance of 5 cm, and same concentration (3 mg/mL) QD@M was irradiated at different laser intensities (0.5-2.5 W/cm²). The temperature changes were recorded by thermal imager. Each experiment was repeated three times. To evaluate photothermal stability of probe, 300 μ L QD@M was irradiated with laser (2 W/cm²) for 10 min and then allowed to cool for 10 min. In photothermal stability test, the system was naturally cooled after laser was irradiated for 10 min to stabilize temperature, the temperature was recorded and same sample was repeated six times. The photothermal conversion efficiency (η) was determined by following equation [39]:

$$\eta = [hS(T_{\max} - T_{\text{surr}}) - Q_{\text{dis}}] / I(1 - 10^{-A_{808}}),$$

I was irradiation power to be 800 mW, A_{808} was absorption of probe at 808 nm (to be 0.89), $T_{\max} - T_{\min}$ was 41 $^{\circ}$ C, τ_s and hS were calculated to be 193.4 s and 6.52; same method measured water (300 μ L) as a control and Q_{dis} was calculated to be 30.84. On the basis of data, η could be obtained.

Biotin-promoted DOX Release

The release kinetics study was carried on by dialysis method, 1 mL QD@M/D-Avidin/FA solution (5 mg/mL) was dispersed in dialysis bag (MW 14000),

and incubated in 20 mL PBS (0.01 M, pH 7.4, pH6.5, pH5.5) at 37 $^{\circ}$ C. At the desired time point, the outside solution was taken out to measure the amount of released DOX *via* fluorescence spectrophotometer. In the experimental group, 0.15 mg biotin was added to the dialysis bag after 3 h of measurement, and 3 mg biotin was also added to the dialysate to maintain the consistency of inside and outside; the control group continued to dialyse without any treatment (n=3).

To evaluate the drug release profile in the cell, HeLa cells were seeded in 6-well plate (5 \times 10⁵ cells per well) and incubated for 24 h at 37 $^{\circ}$ C under 5% CO₂. Cells were treated with fresh culture medium in the presence of QD@M/FITC-Avidin/FA (C_{FITC}=1 μ g/mL) for 2 h and then washed with PBS to remove unbound probe. The cells were continued to culture for desired time and analyzed by FC500 Flow cytometer (Beckman Coulter, USA). Each time point was repeated for 3 times.

In vitro fluorescence imaging

HeLa and A549 cells were seeded in 6-well plate and grown for 24 h. Replaced serum-free medium, QD@M-db/FA and QD@M-db (100 μ g/mL) were cultured with cells for another 2 h. After terminating the culture, cells were washed with PBS for three times to remove free probe. Then cells were immobilized with 4% paraformaldehyde for 30 min and collected for fluorescence imaging.

For confocal imaging of cellular uptake of probe, HeLa and A549 cells were seeded in glass-bottom Petri dishes and incubated for 24 h. The cells were treated with QD@M/D-Avidin/FA and QD@M/D-Avidin (C_{DOX}=1 μ g/mL) for another 2 h. Afterwards, cells were washed with PBS and added 20 μ L DAPI to stain cell nucleus. The intracellular distribution of DOX was observed and imaged by FluoView FV1000 confocal microscopy (Olympus, Japan).

Study of in vitro safety

For *in vitro* comparison of QD@M-db/FA and QD@M-db, MTT assay was used to analysis cell viability of HeLa and A549 cells. Cells were seeded in 96-well plate (1 \times 10⁴ cells per well) and incubated overnight. Subsequently, cells were treated with different amounts of QD@M-db/FA and QD@M-db (12.5, 25, 50, 100 and 200 μ g/mL) for 24 h. After medium was removed, cells were incubated with 20 μ L MTT (5 mg/mL) for another 4 h. The medium was discarded and 150 μ L DMSO was added to each well to solubilize formazan crystal, ELX808IU microplate reader (Biotek, USA) was used to measure the absorption at 490 nm. Untreated cells were used as negative control.

Apoptosis assay

The extent of apoptosis *in vitro* was determined

by Annexin V-FITC/propidium iodide (PI) double staining apoptosis assay. HeLa cells were seeded in 6-well plate and cultured overnight. The cells were transfected by QD@M-DNA/FA or Lipofectamine 2000 at the same concentration of db-DNA (200 nM) for 4 h. After cleaning, they were cultured with DMEM complete medium for another 24 h. At the end point, cells were washed with cooled PBS and suspended in 100 μ L Annexin V binding buffer. 10 μ L Annexin V-FITC and 5 μ L PI were added and incubated at room temperature for 15 min in dark. Each tube was supplemented 400 μ L binding buffer for analysis. Unstained cells and cells stained with Annexin V-FITC or PI were also prepared in parallel. The flow cytometry experiment was repeated for 3 times.

Western blot analysis of inhibition of survivin

To evaluate the inhibition of survivin by db-DNA, above apoptosis cells were subjected to western blot to verify protein reduction. In brief, cells were lysed in cell lysis buffer and collected by centrifugation. The proteins were then separated by 10% SDS-PAGE and electrotransferred onto PVDF membrane. The membrane was blocked with TBST containing 5% nonfat dry milk and then incubated with primary antibody overnight at 4 °C. After washing with TBST, the membrane was hybridized with secondary antibody for 1 h at room temperature. Anti-GAPDH antibody was used as loading control.

Immunohistochemistry (IHC) analysis of inhibition of survivin

To evaluate the inhibition of survivin by db-DNA, HeLa tumor-bearing nude mice were intratumorally injected QD@M-DNA and free DNA, respectively. Tumors were obtained after 24 h, tissue sections were prepared and stained by Cy3 labeled anti-survivin antibody. In IHC, blue was nucleus of DAPI staining and red was survivin labeled by Cy3.

In vitro antitumor therapy

HeLa and A549 cells were seeded in 24-well plate (2×10^5 cells per well) and cultured overnight to analyse PTT *in vitro*. The culture medium was removed and cells were treated with QD@M-db/FA, QD@M-db and QD@M/D-DNA/FA (100 μ g/mL) for 4 h. After washing with PBS to remove unbound probe, each well was added 200 μ L PBS and irradiated with 808 nm laser (2 W/cm²) for 10 min. The cells were stained with calcein and observed under fluorescence microscope.

Combined antitumor therapy in vitro

The combined antitumor therapy was studied

based on MTT assay. HeLa cells were seeded in 96-well plate and cultured overnight. Then cells were exposed to various probes with different concentrations (0.63, 1.25, 2.5 and 5 μ g/mL DOX) for 4 h and irradiated with 808 nm laser (2 W/cm²) for 10 min or without any treatment. Then cells were grown for another 24 h and measured cell viability.

In vivo fluorescence imaging and thermal imaging

4-5 weeks Balb/C nude mice (male, SPF grade) were injected subcutaneously with 100 μ L resuspended HeLa cells (1×10^6) or A549 cells (2×10^6) PBS to induce tumor formation. The tumor began to be treated when its volume reached ~ 100 mm³ ($0.5 \times \text{length} \times \text{width}^2$). For *in vivo* fluorescence imaging, QD@M-db/FA or QD@M-db (60 mg/kg) were administered by tail vein injection in tumor-bearing mice and acquired fluorescence signals at different time points (0, 2, 4, 8, 12, 24 and 48 h). For thermal imaging, HeLa tumor-bearing nude mice were intratumorally injected with PBS (50 μ L) or QD@M-db/FA (50 μ L, 20 mg/mL). 808 nm laser was used to irradiate the tumor site after 24 h of incubation and the temperature was recorded by thermal imager.

In vivo combined antitumor efficacy and safety evaluation

HeLa tumor-bearing nude mice with an average volume of ~ 200 mm³ were randomly divided into five groups (n=6) and intratumorally injected with 50 μ L different probes: (I) PBS, (II) QD@M/D-Avidin/FA, (III) QD@M-DNA/FA, (IV) QD@M/D-DNA/FA and (V) QD@M/D-DNA/FA. 5 injections were done at 1, 5, 9, 13 and 17 d respectively, and group II, III and V were irradiated with 808 nm laser (2 W/cm²) for 10 min at 2 d after the first injection. One mouse from each group was randomly sacrificed after laser irradiation. The tumors were fixed with 4% paraformaldehyde for H&E and IHC staining. The probe concentration was 20 mg/mL, DOX was 600 μ g/mL and db-DNA was 76.4 μ g/mL. The tumor volume and body weight of mice were measured for 30 d. When the experiments were finished, mice were sacrificed and major organs (hearts, livers, spleens, lungs, kidneys and small intestines) were collected, weighed and fixed with 4% paraformaldehyde. Each sample was stained with hematoxylin/eosin (H&E), and then subjected to a microscope to investigate biocompatibility of probe in these tissues. Visceral index was calculated as follows, organ mass/mice mass $\times 100\%$. All animal experiments were approved by Animal Experimental Ethics Committee of Huazhong University of Science and Technology.

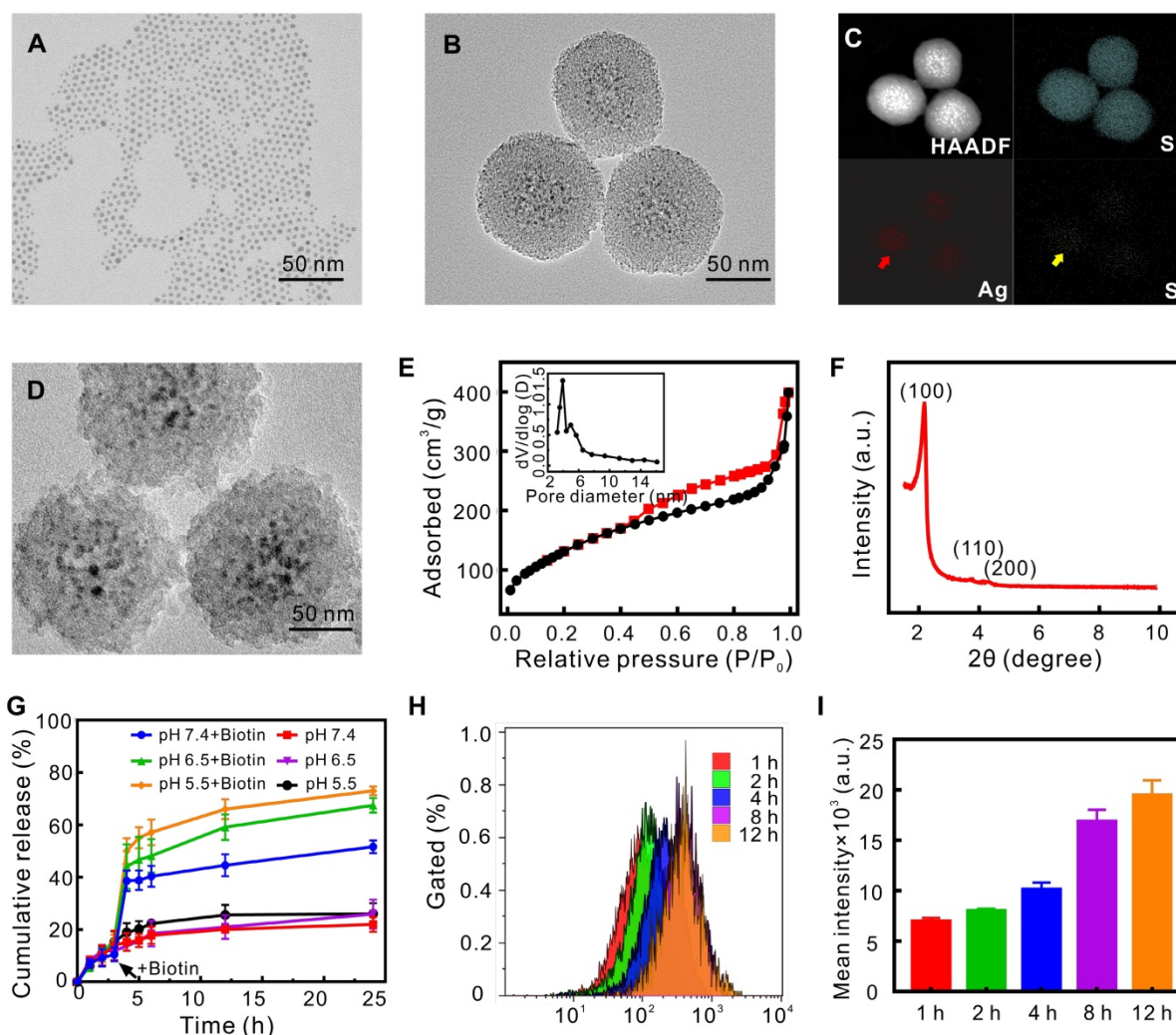


Figure 2. Characterization of nanoparticles and evaluation of drug controlled release capacity. TEM images of Ag₂S QD (A), QD@M (B) and QD@M-DNA/FA (D); high-angle annular dark field image (HAADF), Si, Ag and S elemental mapping images of QD@M (C); nitrogen adsorption-desorption isotherm curve (E) and pore size distribution (inset); small-angle X-ray diffraction of QD@M (F); DOX release curves of QD@M/D-Avidin/FA with and without biotin of different pH (G); intracellular fluorescence intensity (H) and mean intensity (I) were measured by flow cytometry at different time points after QD@M/FITC-Avidin/FA endocytosis in HeLa cells (n=3).

Hemolysis assay

Blood compatibility was evaluated with hemolysis assay. Fresh mice blood was extracted from orbital vein and stabilized with heparin. After accumulating to 2 mL, whole blood was diluted with PBS to 4 mL and centrifuged at 10016 rpm for 5 min to isolate red blood cells (RBCs). The RBCs were further washed and finally diluted to 20 mL PBS. Different concentrations of QD@M-db/FA were incubated with RBCs at 37 °C for 4 h, water as positive control and PBS as negative control. The absorbance of the supernatants from each group was measured using a microplate reader at 570 nm. The hemolysis percentage was calculated as follows:

$$\text{hemolysis percentage} = \frac{(\text{OD}_{\text{test}} - \text{OD}_{\text{negative control}})}{(\text{OD}_{\text{positive control}} - \text{OD}_{\text{negative control}})} \times 100\%$$

Statistics

Statistical analyses were performed by the Student's t-test or one-way analysis of variance (ANOVA) using SPSS 20.0, with significance levels as follows, *: $p < 0.05$, **: $p < 0.01$. Error bars represent standard deviations.

Results and Discussion

Synthesis and characterization of QD@M-DNA/FA

Through the sol-gel reaction, the uniform spherical QD@M nanoparticle (Figure 2B) employed Ag₂S QDs (Figure 2A, 6.5 nm) as core covered by 30-40 nm thick mesoporous silicon as shell, EDX spectrum (Figure S1A) and elemental mapping images (Figure 2C) showed the proportion and distribution of elements. Typical IV type isotherm of N₂

adsorption/desorption isotherm curve (Figure 2E) and small angle XRD pattern (Figure 2F, two-dimensional hexagonal symmetry with space group of $p6mm$) demonstrated an ordered mesoporous characteristic. BET surface area and total pore volume were $602.4 \text{ m}^2/\text{g}$ and $0.51 \text{ cm}^3/\text{g}$ respectively, and the size of whole particle was about 102 nm and pore size calculated by BJH method was 3.29 nm (Figure 2E, inset). We also found that concentrations of Ag_2S and TEOS could affect the shape of QD@M and the thickness of silicon layer, indicating higher concentration of Ag_2S QD would result in thinner silicon layer and adhesion of particles, higher TEOS concentration would result in larger particle and thicker silicon layer (Figure S2). Accordingly, 6 mg Ag_2S QD and 400 μL TEOS were selected to prepare satisfactory dispersible nanoparticle (Figure S1B).

Fluorescence spectrum showed that emission of QD@M was about 1080 nm in NIR-II region under 808 nm excitation, the fluorescence quantum yield was about $3.4 \pm 0.75\%$ (Figure S3A). Owing to the protection of silicon layer, photo-bleaching resistance of Ag_2S QD after encapsulation was improved (Figure S3A, inset). UV-Vis absorbance spectra was used to demonstrate FA modification and DOX loading (Figure S3B), db-modified nitrocellulose membranes (NC membranes) was introduced to confirm that avidin was successfully coupled through desthiobiotin-avidin interaction (Figure S3C, $p < 0.01$). Zeta potential (Figure S3D) and hydrate particle size (Figure S3E) of QD@M/D-DNA/FA were $-21.3 \pm 0.3 \text{ mV}$ and $190.1 \pm 1.17 \text{ nm}$, respectively, the content of Ag_2S in QD@M/D-DNA-FA was calculated to be 7.8% (w/w). The achieved negative charge has been previously shown to be optimal for a long-lasting *in vivo* circulation time. Besides, Carboxyfluorescein (FAM) labeled db-DNA was used to indicate that db-DNA was mainly modified to probe surface by desthiobiotin-avidin interaction, and a small amount was also directly adsorbed by electrostatic adsorption (Figure S3F). Particle stability test illustrated that temperature (in the range of 4–37 °C) and storage environment had little effect on QD@M-DNA/FA (Figure S4). The morphology of QD@M after incubation in DMEM (10% FBS, pH 7.4), PBS of pH 6.5 and pH 5.5 for 30 d was also explored by TEM (Figure S5), the result showed that silicon shell structure was degraded under acidic condition. As tumor was acidic, it provided good microenvironment for the later drug release and degradation of probe.

Ag_2S QD had good photothermal conversion efficiency, and the photothermal ability of QD@M was explored by detecting temperature changes under 808 nm laser irradiation. The results showed that photothermal effect of QD@M was concentration

dependent (Figure S6A, C) and laser power intensity dependent character (Figure S6B, D). More importantly, QD@M did not show significant decrease in photothermal conversion after continuous laser irradiation for six cycles (Figure S6E). The photothermal conversion efficiency (η) of QD@M was 33.86% (Figure S6F). TEM results also revealed that silicon shell skeleton did not scatter, and still maintained core-shell structure (Figure S7), showing an ideal photostability of QD@M. Therefore, QD@M had an outstanding photothermal effect and photostability for PTT.

Biotin-dependent drug release

In our targeting drug delivery system, avidin was used as a “gatekeeper” to control drug and db-DNA release. As the affinity of biotin toward avidin was higher than that of db, biotin would replace db and competitively bind avidin, making it leave from pore entrance and release the drug in pore, and dissociate db-DNA from avidin too. Here, DOX was adsorbed into pore, the loading rate and encapsulation efficiency reached up to $2.87 \pm 0.13\%$ and $51.33 \pm 5.79\%$, respectively. To investigate the controlled release behavior of our designed system, drug release effect in the presence and absence of biotin *in vitro* was simulated under different pH conditions (Figure 2G). Under acidic conditions that mimicked the tumor microenvironment (pH 6.5 and pH 5.5), the release rate of each group was about 10% at 3 h before biotin was added; in the presence of biotin, the cumulative release of DOX from QD@M/D-Avidin/FA was increased significantly to about $67.44 \pm 2.73\%$ (pH 6.5) and $72.94 \pm 1.723\%$ (pH 5.5), respectively, at 24 hours posttreatment, which was higher than that without biotin (approximately 25%). The release profiles of DOX from QD@M/D-Avidin/FA in neutral buffer (pH 7.4) were also examined, the release profiles similar to those observed under acidic conditions. Moreover, the cumulative release of DOX under acidic conditions showed an increased compared with that under neutral condition. Tumor tissue was under acidic pH and express maximal biotin to trigger the release of DOX. When drug-loaded probe entered into tumor cell, drug could be released rapidly under the both stimulations to achieve killing ability of drug. To verify this speculation, QD@M/FITC-Avidin/FA was prepared by loading fluorescein isothiocyanate (FITC) instead of DOX. Flow cytometry was used to detect fluorescence intensity of FITC in cell which was continuously cultured for different time slot (Figure 2H, I). It was found that intracellular fluorescence gradually increased with time and stabilized after 8 h. Because the fluorescence of FITC in pore was inhibited since

Ag₂S QD affected the fluorescence of nearby fluorescent dye, and the recovery of FITC fluorescence was the indication of its release from pore into cytoplasm. Taken together, our smart drug delivery system exhibited an effective control of drug release and presented great potential for tumor therapy.

FA receptor-mediated endocytosis of QD@M/D-Avidin/FA

Firstly, the NIR-II fluorescence imaging property of QD@M was investigated. It was found that when the concentration increased, the fluorescence intensity enhanced gradually, indicating that the fluorescence of QD@M was concentration-dependent (Figure 3A).

Efficient cellular uptake was an essential requirement for treatment efficacy of multifunctional nanoparticle. Modifying the targeting ligand on surface of nanoparticle was an effective way to increase probe uptake by receptor-mediated endocytosis. To test targeting specificity of probe, HeLa and A549 cells with high and low expression of FA receptor were used as positive and negative cells, respectively. QD@M-db/FA and QD@M/D-Avidin/FA were used as positive probes, while no FA-coupled QD@M-db and QD@M/D-Avidin were used as negative probes. After these probes were incubated with both cells for 2 h, NIR-II fluorescence images revealed that HeLa cells incubated with QD@M-db/FA exhibited the strongest fluorescence signal (Figure 3B), significantly higher than other groups. Although A549 cells incubated with QD@M-db/FA also had weak fluorescence, which should be caused by non-specific adsorbed probe. Confocal images showed that QD@M/D-Avidin/FA transported the most DOX into

HeLa cells (Figure 3C), and the red fluorescence signal of DOX was mainly distributed in cytoplasm, a few into nucleus because of the short incubation time. While there was a certain amount of red fluorescence in A549 cells incubated with QD@M/D-Avidin/FA, and the other two groups were very few, confirming that FA-modified probe was subject to FA receptor-mediated endocytosis. In consequence, FA-modified multifunctional probe had excellent targeting properties. Besides, the above-mentioned experimental cells continued to be cultured for 6h and 12h after treatment and washing. With the release of DOX triggered by biotin in cells, DOX began to enter nucleus after 6h and most drugs entered the nucleus after 12 h of treatment (Figure S8). The intracellular release and treatment of the drug were studied.

As a potential drug delivery system, biocompatibility of probe was the key to assessment. HeLa and A549 cells were incubated with different concentrations of QD@M-db/FA or QD@M-db for 24 h, respectively. MTT results showed that survival rate of HeLa cells remained $68.5\pm 3.4\%$ when QD@M-db/FA concentration reached $200\ \mu\text{g}/\text{mL}$, and that of A549 cells was $86.3\pm 4.1\%$, probably due to the uptake of more targeting probe by HeLa cells (Figure 3D, E). It was also found that the targeting property of probe had an effect on cell survival. After incubation of HeLa cells with $200\ \mu\text{g}/\text{mL}$ QD@M-db/FA and QD@M-db, cell survival rate of probe with FA ligand was lower than that of probe without FA ligand ($77.6\pm 13.5\%$), whereas there was no significant difference in cell survival rate for A549 cells incubation with different probes.

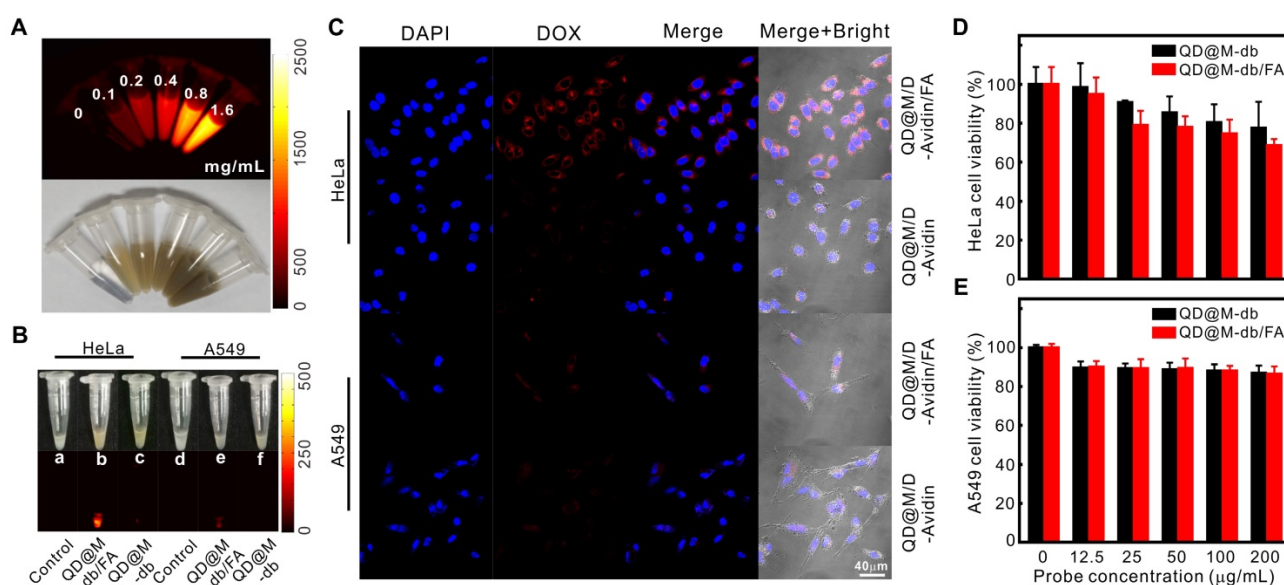


Figure 3. Targeting and *in vitro* biocompatibility of probes. Fluorescence and white light images of QD@M at different concentrations (A); NIR fluorescence images of HeLa and A549 cells incubated with QD@M-db/FA and QD@M-db (B); confocal fluorescence images of HeLa and A549 cells incubated with QD@M/D-Avidin/FA and QD@M/D-Avidin (C); survival of HeLa (D) and A549 (E) cells incubated with QD@M-db/FA and QD@M-db at different concentrations.

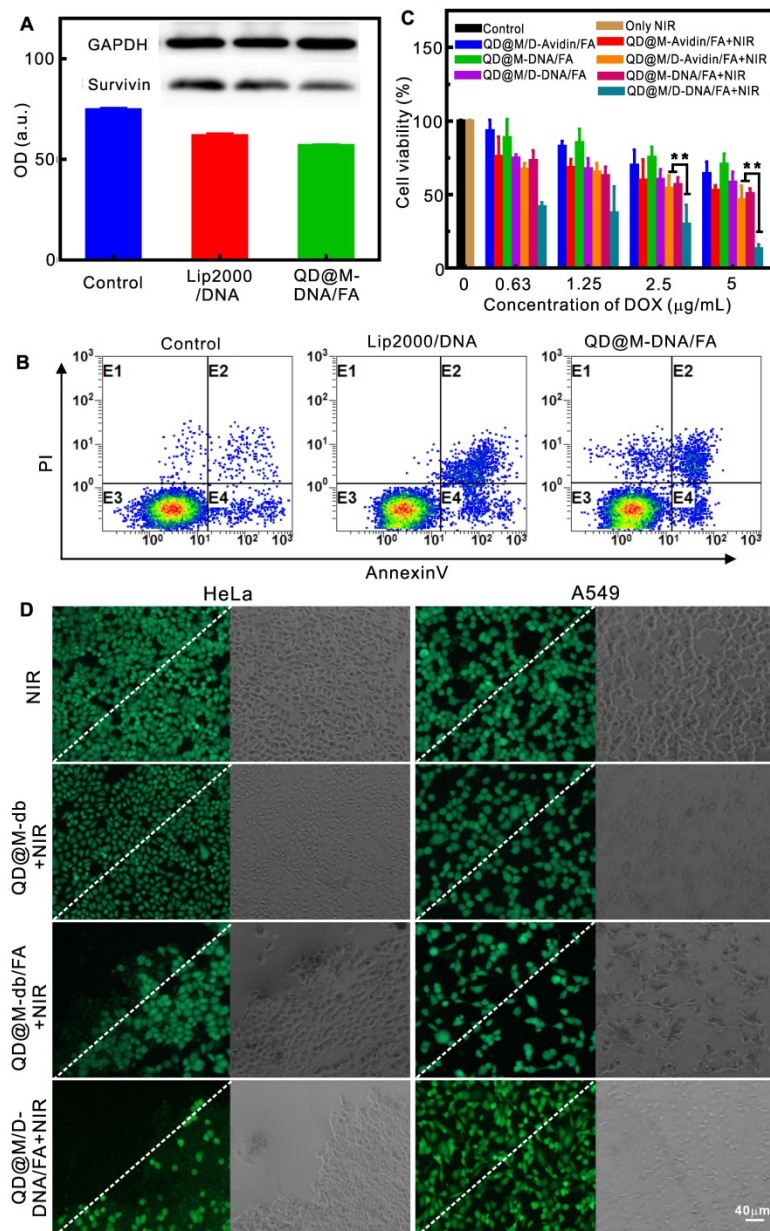


Figure 4. Evaluation of the therapy effect *in vitro*. Western blot analysis of intracellular survivin protein after Lip 2000 and QD@M-DNA/FA transfected antisense oligonucleotide (A); flow cytometry of the apoptosis induced by Lip 2000 and QD@M-DNA/FA transfection of antisense oligonucleotide (B) (n=3); MTT assay of survival rate of HeLa cells treated with different probes (C); fluorescence imaging of calcein staining HeLa and A549 cells irradiated by laser (2 W/cm²) for 10 min after incubation with QD@M-db, QD@M-db/FA and QD@M/D-DNA/FA for 2 h (D), the white dashed line was the irradiation boundary. **: p<0.01.

Investigation on *in vitro* antitumor effect

The treatment of tumor by multifunctional nanoplatform QD@M/D-DNA/FA included three parts: chemotherapy, photothermal therapy and apoptosis of survivin antisense oligonucleotide. To verify the ability of probe to deliver nucleic acid, QD@M-DNA/FA and commercialized Lip 2000 were compared to transfect survivin antisense oligonucleotide. The expression of survivin protein in HeLa cells were detected by western blot (Figure 4A), and both of them had almost the same gene silencing effect on survivin. Flow cytometry was also used to examine apoptosis by using Annexin V-FITC and PI

double staining (Figure 4B). DNA-loaded QD@M-DNA/FA treated group yielded approximately 14.7% apoptosis induction rate, and similar with Lip2000 treatment (16.9%), demonstrating that this DNA deliver system could knockdown gene expression and induce apoptosis as an adjuvant therapy. In addition, immunohistochemistry (IHC) was used to analyze the survivin inhibitions in QD@M-DNA/FA and free DNA treated tumors, and it was found that the inhibition of survivin was better when DNA was delivered into tissue cells by QD@M-DNA/FA probe (Figure S9).

Previous studies confirmed that tumor cell

would necrosis due to heat-induced protein denaturation when temperature exceeded 50 °C, and our probe with low concentration showed the potential of cell photothermal therapy under 808 nm laser irradiation (Figure S10), so the photothermal effect of our probe in cells was also assessed. The results showed that HeLa cells incubated with QD@M-db/FA exhibited obvious cell death after staining with calcein (Figure 4D), while the same treatment by negative QD@M-db without FA ligand showed no apparent cell death. In addition, no cell death occurred in A549 cells, and laser irradiation alone could not kill tumor cell. Hence, the targeting probe designed by us had excellent targeting property and good PTT effect on FA receptor high expression tumor cell. Furthermore, the HeLa cell treated with QD@M/D-DNA/FA showed cell death in laser irradiated area and partial apoptosis in non-irradiated area due to the action of DOX and antisense oligonucleotide.

The combined therapeutic effect of QD@M/D-DNA/FA on HeLa cells was evaluated by MTT assay (Figure 4C). It should be noted that since unit probe carried a certain amount of drug, DOX concentration here indicated probe concentration. In accordance with photothermal fluorescence imaging (Figure 4D), laser irradiation alone had no effect on cell survival. The results revealed that in the absence of laser irradiation, when DOX, oligonucleotide or both were delivered to cells, survival rate decreased gradually with the increase of probe concentration; as its concentration reached 5 µg/mL, cell survival rates decreased to 64.03±8.11, 70.42±7.39 and 58.11±7.18%, respectively. Comparison of these results showed that antisense oligonucleotide had the weakest killing effect on tumor cell, which was due to its low apoptosis efficiency, and synergistic effect of the two modes of action was relatively better. Under laser irradiation, 5 µg/mL QD@M-Avidin/FA without DOX and antisense oligonucleotide could reduce cell survival to 52.63±3.45% owing to its good PTT effect. Meanwhile, once PTT was combined with DOX or antisense oligonucleotide, the lower concentration of probe (0.63 µg/mL) exhibited high cytotoxicity (67.1±4.1 and 72.98±7.03%). This trend was more obvious at high concentration. When probe concentration reached up to 5 µg/mL, survival rates of cells combined laser irradiation with DOX or antisense oligonucleotide were 46.2±9.8 and 50.6±3.3%, while the combination of the three was only 13.04±2.77%, which was significantly different compared with the former two ($p < 0.01$) (Figure 4C). Together, the above results proved that the synergistic effect of QD@M/D-DNA/FA carrying DOX and survivin antisense oligonucleotide under laser irradiation was superior

to other treatment groups in tumor cell therapy.

In vivo targeted NIR fluorescence imaging and antitumor therapy

Due to high NIR fluorescence quantum yield of Ag₂S QD, fluorescence imaging performance of probe targeting tumor *in vivo* was further investigated. QD@M-db/FA was injected into HeLa tumor-bearing nude mice through tail vein (Figure 5B). Fluorescence signal began to enhance at the tumor site after 2 h, and continued to increase over time. The signal was brightest during 8-12 h and could still be observed after 48 h. To assess the targeting ability of probe *in vivo*, HeLa and A549 tumor-bearing nude mice were intravenously injected with same concentration of QD@M-db/FA and QD@M-db, respectively. As shown in Figure S11, compared with other experimental groups, FA ligand-modified QD@M-db/FA exhibited the strongest signal and more persistent enrichment for HeLa tumor (high FA receptor expression), indicating that our targeting probe was an excellent fluorescence tracer probe owing to its strong fluorescence signal and long residence time at tumor site.

Encouraged by the excellent synergistic therapeutic effect in cell experiments of probe, the combined tumor therapy of probe was further carried out *in vivo*. To verify the potential of probe to induce hyperthermia effect *in vivo*, tumor was injected with PBS or QD@M-db/FA, and the temperature of both increased under laser irradiation (Figure 5C). After 10 min exposure, the temperature reached to 41.2 and 54.4 °C, respectively (Figure 5D), the latter temperature could be sufficient to kill tumor cells while the former was harmless to tumor. For purpose of improving therapeutic effect, HeLa tumor-bearing nude mice were intratumorally injected with different probes for 5 times every 4 d [40,41], and in order to take maximum advantage of DOX and antisense oligonucleotide, laser irradiation was administered at 24 h after the first injection (Figure 5A). Analyzing the change in tumor volume (Figure 5E), it was found the group of QD@M/D-DNA/FA without laser irradiation showed moderate inhibition of tumor growth compared with control group due to synergistic effect of chemotherapy and gene therapy. In the experimental group irradiated by laser, the tumor tissues all suffered scab formation and exfoliation after heating up (Figure 5H). Unfortunately, group III mice treated with photothermal and gene therapy began to recur at 8 d and the similar phenomenon occurred in group II at 10 d which dealt with chemo-photothermal therapy (Figure 5E). Moreover, all the mice in these two groups relapsed and tumor volume began to increase continuously, illustrating

that tumor therapeutic effect of combining photothermal with gene therapy or chemotherapy was not satisfactory. It could also be found that tumor volume in group III grew faster than that in group II ($p < 0.05$), which was consistent with the experimental result at cellular level that gene therapy was less effective than chemotherapy. This phenomenon might be caused by the partial degradation of antisense oligonucleotide, which affected gene silencing efficiency. Moreover, photothermal heating could increase the permeability of cell membrane, promoting endocytosis of probe and inducing drug release, thus improved chemotherapy effect. Excitingly, the mice injected with co-delivery system QD@M/D-DNA/FA coupled with laser irradiation (group V) obtained the most efficient antitumor effect. Only one mouse regrew tumor after 20 d in the whole experimental period, and there was significant difference between group V and group III ($p < 0.01$) in inhibiting tumor growth, also for group II ($p < 0.05$). The excellent antitumor effect achieved here might be due to the synergistic treatment of chemo-, gene-, and photothermal therapeutic effect. The same results

were also found in H&E and IHC staining sections of tumors from each treatment group (Figure S12). Compared with the non-irradiated group IV, the laser-irradiated groups had a larger area of cell necrosis; compared with the control group, the experimental groups had inhibitory effect on survivin expression, while the group II without gene therapy had less inhibitory effect than other treatment groups. Mice were sacrificed after 30 d treatment and tumor masses were measured to calculate tumor index (Figure 5G, tumor index=tumor weight/body weight $\times 100\%$). Similar to the previous results, the combined effect of chemo-, gene and photothermal therapy was significantly better than those of other groups ($p < 0.05$ or $p < 0.01$). In addition, no noticeable body weight loss was observed in all groups during treatment process (Figure 5F), indicating outstanding biocompatibility of probe and the treatment had no obvious toxicity to mice. All in all, above results demonstrated that QD@M/D-DNA/FA combined with laser irradiation achieved significant therapeutic effect and prolonged the prognosis.

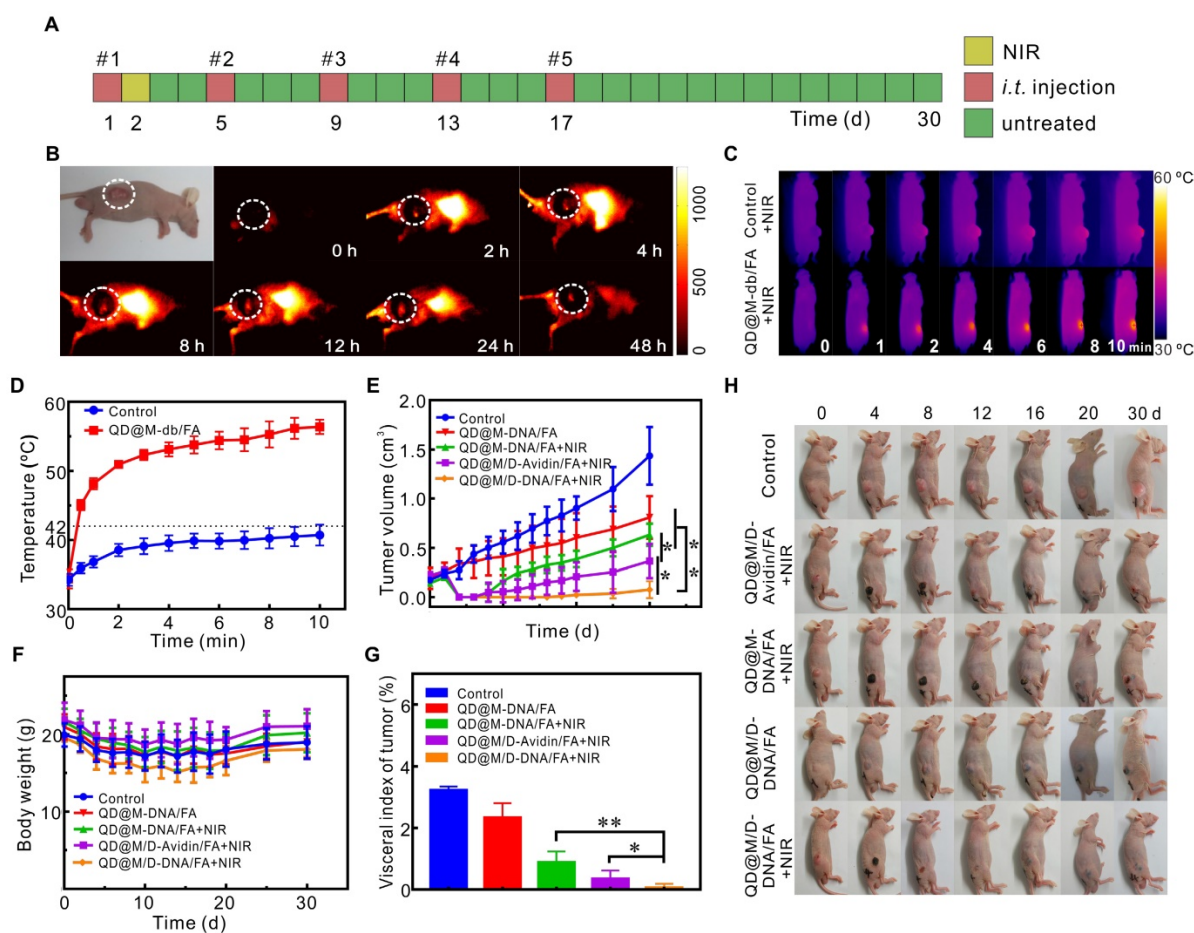


Figure 5. The fluorescence imaging and tumor treatment *in vivo*. Schematic illustration of treatment route (A); fluorescence imaging at different time points after tail vein injection of QD@M-db/FA into HeLa tumor-bearing nude mice (B); infrared thermal imaging results (C) and temperature variation curves (D) of tumor site irradiated by laser after intratumoral injection of PBS and QD@M-db/FA for 24 h; tumor growth after different treatments (E); body weights (F) and images (H) of mice with various treatments during 30 d; ratio of tumor mass to body weight in different groups at end of treatment (G). $n=5$, *, $p < 0.05$, **, $p < 0.01$.

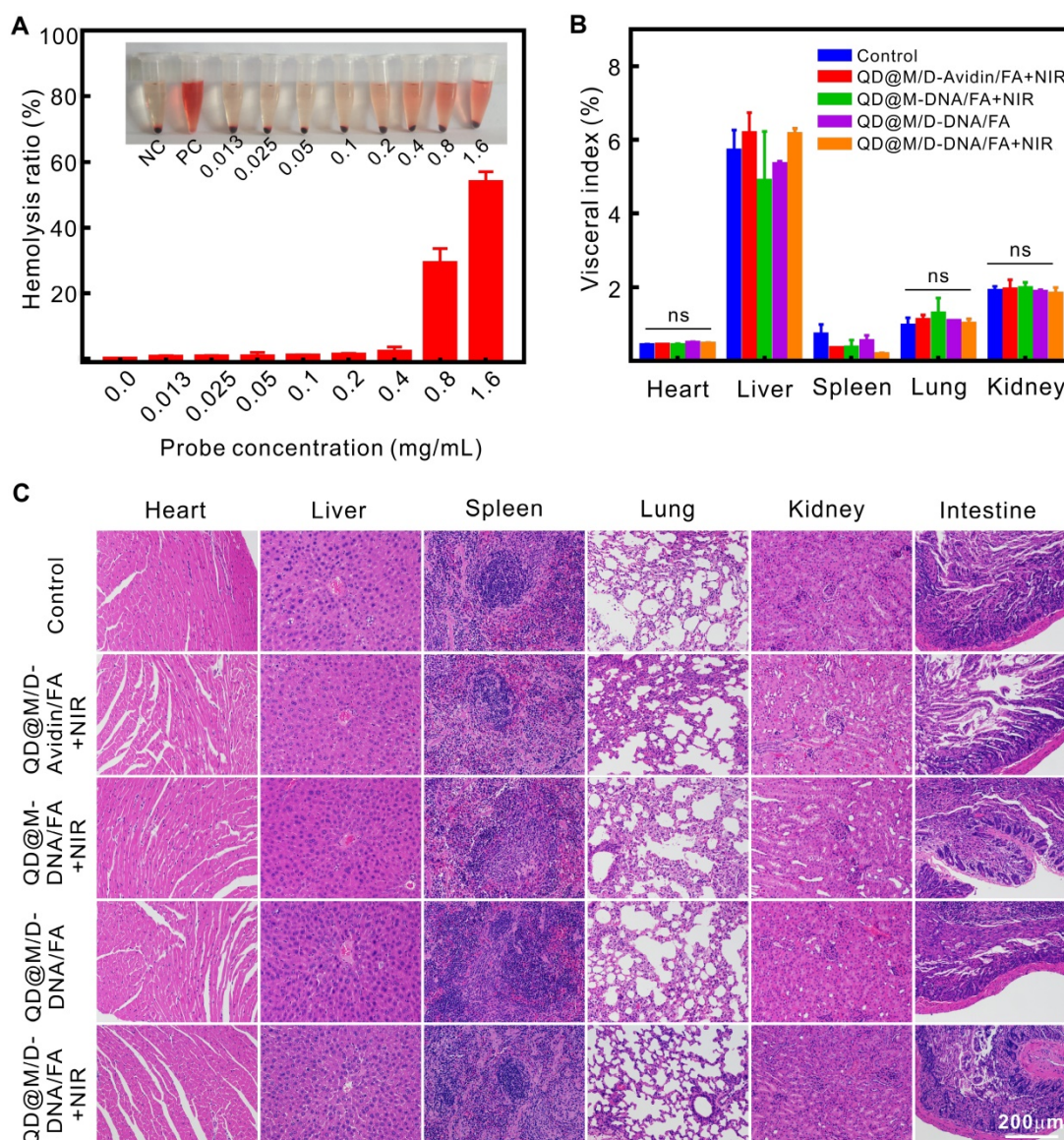


Figure 6. Evaluation of blood compatibility and biological safety. Hemolysis of QD@M-FA (A); visceral index of major organs at the end of different treatment groups (B); H&E staining of major organs at the end of different treatment groups (C). ns: no statistical significance.

In vivo biocompatibility and safety

The excellent multifunctional nanoplatform not only needed stable imaging and high-efficiency therapeutic effect, but also required satisfactory biosecurity *in vivo*. Since probe needed to participate in blood circulation after injection, hemolysis by nanoparticle was a crucial consideration. The result showed that slight hemolysis began to occur when the concentration of QD@M-db/FA as high as 0.8 mg/mL (Figure 6A), suggesting that tail vein injection of probe could be nontoxic toward erythrocyte *in vivo*.

The toxicity of tumor therapy on mice was evaluated by comparing organ index and H&E staining of each group after treatment. Visceral index was the ratio of viscera weight and body weight, it was relatively constant under normal condition, and it

would change while organ was damaged, the increase of visceral index indicated congestion, edema or hyperplasia, and decrease illustrated organ atrophy or other degenerative diseases. The data revealed that there was no apparent difference in heart, lung and kidney index between control group and experimental group (Figure 6B), there might be a little damage in liver and spleen since both visceral index slightly increased or decreased. As liver and spleen were the main metabolic or immune organ, it was speculated that liver and spleen captured and enriched probe which leading to the slight abnormality. The enrichment phenomena could be certified in fluorescence imaging (Figure 5B). Compared to the control group, neither noticeable damage nor inflammation was observed from H&E staining images of major organs (Figure 6C). The heart did not present reduction of

fibrosis or vacuolation, pulmonary alveoli was significant without fibrosis or congestion, and clear and complete glomerular structure could be seen in kidneys. In conclusion, the drug delivery system for combination therapy could greatly suppress tumor growth without any apparent side effect.

Conclusions

In summary, a multifunctional nanoplatform (QD@M/D-DNA/FA) with the ability of tumor targeting fluorescence imaging and combining chemotherapy, PTT and gene therapy was successfully designed and constructed. The probe employed Ag₂S QD with NIR-II fluorescence and photothermal properties as core covered by mesoporous silica as shell. The pore loaded with drug was capped by desthiobiotin-avidin complex, survivin antisense oligonucleotide and FA were grafted onto the probe surface for gene therapy and targeting tumor. *In vitro* and *in vivo* experiments proved that the probe had satisfactory biocompatibility and targeting fluorescence imaging ability, and could effectively inhibit tumor growth under the synergistic effect of biotin-responsive drug controlled release, PTT and gene-induced apoptosis. This novel theranostic platform combined synergistic therapy and real-time imaging might hold promise for efficient tumor therapy.

Abbreviations

Ag(DDTC): Diethyldithiocarbamic acid silver salt; APTES: 3-aminopropyltriethoxysilane; CTAB: hexadecyltrimethylammonium bromide; db: desthiobiotin; DOX: doxorubicin; FA: folic acid; FAM: carboxyfluorescein; H&E: hematoxylin/eosin; IHC: immunohistochemistry; MSN: mesoporous silica nanoparticle; NC: nitrocellulose membranes; QDs: quantum dots; PTT: photothermal therapy; PDI: polydispersity index; SDS-PAGE: sodium dodecyl sulphate-polyacrylamide gel electrophoresis; TEOS: tetraethylorthosilicate.

Supplementary Material

Supplementary figures.

<http://www.thno.org/v08p5662s1.pdf>

Acknowledgments

This work was supported by the National Key Research and Development Program of China (2017YFA0700501), the National Natural Science Foundation of China (Grant No. 81471697, 81771878), and the Fundamental Research Funds for the Central Universities (Hust: 2016YXMS253, 2017KFXKJC002, 2018KFYXKJC048). We also thank the Analytical and Testing Center (HUST) and the Center for Nanoscale

Characterization & Devices (CNCD) at WNLO of HUST for the help of measurement.

Competing Interests

The authors have declared that no competing interest exists.

References

1. Thun MJ, DeLancey JO, Center MM, Jemal A, Ward EM. The global burden of cancer: priorities for prevention. *Carcinogenesis*. 2009; 31: 100-10.
2. Fan W, Yung B, Huang P, Chen X. Nanotechnology for multimodal synergistic cancer therapy. *Chem Rev*. 2017; 117: 13566-638.
3. Hong G, Antaris AL, Dai H. Near-infrared fluorophores for biomedical imaging. *Nat Biomed Eng*. 2017; 1: 0010.
4. Chen G, Tian F, Zhang Y, Zhang Y, Li C, Wang Q. Tracking of transplanted human mesenchymal stem cells in living mice using near-infrared Ag₂S quantum dots. *Adv Funct Mater*. 2014; 24: 2481-8.
5. Li C, Li F, Zhang Y, Zhang W, Zhang X-E, Wang Q. Real-time monitoring surface chemistry-dependent *in vivo* behaviors of protein nanocages via encapsulating an NIR-II Ag₂S quantum dot. *ACS Nano*. 2015; 9: 12255-63.
6. Li C, Zhang Y, Wang M, Zhang Y, Chen G, Li L, et al. *In vivo* real-time visualization of tissue blood flow and angiogenesis using Ag₂S quantum dots in the NIR-II window. *Biomaterials*. 2014; 35: 393-400.
7. Du Y, Xu B, Fu T, Cai M, Li F, Zhang Y, et al. Near-infrared photoluminescent Ag₂S quantum dots from a single source precursor. *J Am Chem Soc*. 2010; 132: 1470-1.
8. Sadovnikov S, Gusev A. Recent progress in nanostructured silver sulfide: from synthesis and nonstoichiometry to properties. *J Mater Chem A Mater*. 2017; 5: 17676-704.
9. Jiang P, Tian Z-Q, Zhu C-N, Zhang Z-L, Pang D-W. Emission-tunable near-infrared Ag₂S quantum dots. *Chem Mater*. 2011; 24: 3-5.
10. Yang T, Tang Ya, Liu L, Lv X, Wang Q, Ke H, et al. Size-dependent Ag₂S nanodots for second near-infrared fluorescence/photoacoustics imaging and simultaneous photothermal therapy. *ACS Nano*. 2017; 11: 1848-57.
11. Zhang Y, Hong G, Zhang Y, Chen G, Li F, Dai H, et al. Ag₂S quantum dot: a bright and biocompatible fluorescent nanoprobe in the second near-infrared window. *ACS Nano*. 2012; 6: 3695-702.
12. Hong G, Robinson JT, Zhang Y, Diao S, Antaris AL, Wang Q, et al. *In vivo* fluorescence imaging with Ag₂S quantum dots in the second near-infrared region. *Angew Chem Int Ed Engl*. 2012; 124: 9956-9.
13. Qin M-Y, Yang X-Q, Wang K, Zhang X-S, Song J-T, Yao M-H, et al. *In vivo* cancer targeting and fluorescence-CT dual-mode imaging with nanoprobes based on silver sulfide quantum dots and iodinated oil. *Nanoscale*. 2015; 7: 19484-92.
14. Lu N, Huang P, Fan W, Wang Z, Liu Y, Wang S, et al. Tri-stimuli-responsive biodegradable theranostics for mild hyperthermia enhanced chemotherapy. *Biomaterials*. 2017; 126: 39-48.
15. Hauck TS, Jennings TL, Yatsenko T, Kumaradas JC, Chan WC. Enhancing the toxicity of cancer chemotherapeutics with gold nanorod hyperthermia. *Adv Mater*. 2008; 20: 3832-8.
16. Kim H, Kim WJ. Photothermally controlled gene delivery by reduced graphene oxide-polyethylenimine nanocomposite. *Small*. 2014; 10: 117-26.
17. Wang C, Xu L, Liang C, Xiang J, Peng R, Liu Z. Immunological responses triggered by photothermal therapy with carbon nanotubes in combination with anti-CTLA-4 therapy to inhibit cancer metastasis. *Adv Mater*. 2014; 26: 8154-62.
18. Wang T, Wang D, Yu H, Wang M, Liu J, Feng B, et al. Intracellularly acid-switchable multifunctional micelles for combinational photo/chemotherapy of the drug-resistant tumor. *ACS Nano*. 2016; 10: 3496-508.
19. Wei T, Liu J, Ma H, Cheng Q, Huang Y, Zhao J, et al. Functionalized nanoscale micelles improve drug delivery for cancer therapy *in vitro* and *in vivo*. *Nano Lett*. 2013; 13: 2528-34.
20. Fiandra L, Mazzucchelli S, De Palma C, Colombo M, Allevi R, Sommaruga S, et al. Assessing the *in vivo* targeting efficiency of multifunctional nanoconstructs bearing antibody-derived ligands. *ACS Nano*. 2013; 7: 6092-102.
21. Meng H, Mai WX, Zhang H, Xue M, Xia T, Lin S, et al. Codelivery of an optimal drug/siRNA combination using mesoporous silica nanoparticles to overcome drug resistance in breast cancer *in vitro* and *in vivo*. *ACS Nano*. 2013; 7: 994-1005.
22. Murata M, Narahara S, Kawano T, Hamano N, Piao JS, Kang J-H, et al. Design and function of engineered protein nanocages as a drug delivery system for targeting pancreatic cancer cells via neuropilin-1. *Mol Pharm*. 2015; 12: 1422-30.
23. Kecht J, Schlossbauer A, Bein T. Selective functionalization of the outer and inner surfaces in mesoporous silica nanoparticles. *Chem Mater*. 2008; 20: 7207-14.
24. Li Z, Barnes JC, Bosoy A, Stoddart JF, Zink JI. Mesoporous silica nanoparticles in biomedical applications. *Chem Soc Rev*. 2012; 41: 2590-605.

25. Meng H, Xue M, Xia T, Ji Z, Tarn DY, Zink JL, et al. Use of size and a copolymer design feature to improve the biodistribution and the enhanced permeability and retention effect of doxorubicin-loaded mesoporous silica nanoparticles in a murine xenograft tumor model. *ACS Nano*. 2011; 5: 4131-44.
26. Kim J, Kim HS, Lee N, Kim T, Kim H, Yu T, et al. Multifunctional uniform nanoparticles composed of a magnetite nanocrystal core and a mesoporous silica shell for magnetic resonance and fluorescence imaging and for drug delivery. *Angew Chem Int Ed Engl*. 2008; 47: 8438-41.
27. An J, Yang XQ, Cheng K, Song XL, Zhang L, Li C, et al. In vivo computed tomography/photoacoustic imaging and NIR-triggered chemo-photothermal combined therapy based on a gold nanostar-, mesoporous silica-, and thermosensitive liposome-composited nanoprobe. *ACS Appl Mater Interfaces*. 2017; 9: 41748-59.
28. Fan W, Shen B, Bu W, Chen F, Zhao K, Zhang S, et al. Rattle-structured multifunctional nanotheranostics for synergetic chemo-/radiotherapy and simultaneous magnetic/luminescent dual-mode imaging. *J Am Chem Soc*. 2013; 135: 6494-503.
29. Zhao Z, Meng H, Wang N, Donovan MJ, Fu T, You M, et al. A controlled-release nanocarrier with extracellular pH value driven tumor targeting and translocation for drug delivery. *Angew Chem Int Ed Engl*. 2013; 52: 7487-91.
30. Ma X, Nguyen KT, Borah P, Ang CY, Zhao Y. Functional silica nanoparticles for redox-triggered drug/ssDNA co-delivery. *Adv Healthc Mater*. 2012; 1: 690-7.
31. Huo M, Wang L, Chen Y, Shi J. Tumor-selective catalytic nanomedicine by nanocatalyst delivery. *Nat Commun*. 2017; 8: 357.
32. Zhang M, Xu C, Wen L, Han MK, Xiao B, Zhou J, et al. A hyaluronidase-responsive nanoparticle-based drug delivery system for targeting colon cancer cells. *Cancer Res*. 2016; 76: 7208-18.
33. Ma X, Sreejith S, Zhao Y. Spacer intercalated disassembly and photodynamic activity of zinc phthalocyanine inside nanochannels of mesoporous silica nanoparticles. *ACS Appl Mater Interfaces*. 2013; 5: 12860-8.
34. Russell-Jones G, McTavish K, McEwan J, Rice J, Nowotnik D. Vitamin-mediated targeting as a potential mechanism to increase drug uptake by tumours. *J Inorg Biochem*. 2004; 98: 1625-33.
35. Chivers CE, Crozat E, Chu C, Moy VT, Sherratt DJ, Howarth M. A streptavidin variant with slower biotin dissociation and increased mechanostability. *Nat Methods*. 2010; 7: 391.
36. Wu M, Meng Q, Chen Y, Zhang L, Li M, Cai X, et al. Large pore-sized hollow mesoporous organosilica for redox-responsive gene delivery and synergistic cancer chemotherapy. *Adv Mater*. 2016; 28: 1963-9.
37. Ambrosini G, Adida C, Altieri DC. A novel anti-apoptosis gene, survivin, expressed in cancer and lymphoma. *Nat Med*. 1997; 3: 917.
38. Schlossbauer A, Kecht J, Bein T. Biotin-avidin as a protease-responsive cap system for controlled guest release from colloidal mesoporous silica. *Angew Chem Int Ed Engl*. 2009; 121: 3138-41.
39. Roper DK, Ahn W, Hoepfner M. Microscale heat transfer transduced by surface plasmon resonant gold nanoparticles. *J Phys Chem C Nanomater Interfaces*. 2007; 111: 3636-41.
40. Duan S, Yang Y, Zhang C, Zhao N, Xu FJ. NIR-responsive polycationic gatekeeper-cloaked hetero-nanoparticles for multimodal imaging-guided triple-combination therapy of cancer. *Small*. 2017; 13: 1603133.
41. Meng Y, Wang S, Li C, Qian M, Yan X, Yao S, et al. Photothermal combined gene therapy achieved by polyethyleneimine-grafted oxidized mesoporous carbon nanospheres. *Biomaterials*. 2016; 100: 134-42.